

Spin injection/detection using an organic-based magnetic semiconductor

Jung-Woo Yoo^{1,2}, Chia-Yi Chen³, H. W. Jang⁴, C. W. Bark⁴, V. N. Prigodin¹, C. B. Eom⁴
and A. J. Epstein^{1,2*}

The new paradigm of electronics, 'spintronics', promises to extend the functionality of information storage and processing in conventional electronics¹. The principal spintronics device, the 'spin valve', consists of two magnetic layers decoupled by a spin-transporting spacer, which allows parallel (on) and antiparallel (off) alignment of the magnetizations (spins) of the two magnetic layers. The device resistance then depends on the spin alignment controlled by the external magnetic field. In pursuit of semiconductor spintronics², there have been intensive efforts devoted to develop room-temperature magnetic semiconductors³ and also to incorporate both inorganic semiconductors⁴ and carbon-based materials^{5–11} as the spin-transporting channels. Molecule/organic-based magnets, which allow chemical tuning of electronic and magnetic properties, are a promising new class of magnetic materials for future spintronic applications^{12,13}. Here, we report the realization of an organic-based magnet as an electron spin polarizer in the standard spintronics device geometry. A thin non-magnetic organic semiconductor layer and an epitaxial ferromagnetic oxide film were employed to form a hybrid magnetic tunnel junction. The results demonstrate the spin-polarizing nature of the organic-based magnetic semiconductor, vanadium(TCNE: tetracyanoethylene)_x ($x \sim 2$; $T_c \sim 400$ K), and its function as a spin injector/detector in hybrid magnetic multilayer devices.

Molecule/organic-based magnets are relatively new materials created by chemical synthesis targeting magnetic properties at the macroscopic and/or molecular level. These materials, ranging from solely organic to organic/inorganic hybrid complexes, exhibit scientific richness in both physics and chemistry. The flexibility of organic chemical methodology, which can adjust molecular units within these systems, introduces tunability of tailor-made magnetic and electronic properties¹². The presence of large molecular units generally leads to a low spin density, which makes these materials difficult to use in practical applications of conventional magnets. However, strong on-site Coulomb interaction together with 'weak' intermolecular overlapping within these materials can lead to highly spin-polarized bands with a relatively narrow bandwidth¹³. This anticipation of high spin polarization in metal-(TCNE) magnets has been broadly supported by both experimental studies^{14–16} and theoretical calculations^{16–18} indicating that these materials are promising candidates for future spintronics applications. An intriguing challenge arises concerning whether these materials can be incorporated into the platform of conventional magnetic multilayer devices.

$V(\text{TCNE})_x$ ($x \sim 2$, magnetic ordering temperature (T_c) ~ 400 K) is the earliest developed room-temperature molecule-based magnet¹⁹. The magnetic order of this material is due to direct exchange coupling (J) between the unpaired electrons in the π^* orbitals of $(\text{TCNE})^-$ anions, in which the spins are distributed over the entire anions²⁰, and the spins in the transition metal V^{II} ions. J is antiferromagnetic, yielding a net magnetic moment $\sim 1 \mu_B$ from the antiparallel configuration between spins in two $(\text{TCNE})^-$ anions (each $S = 1/2$) and one V^{II} ($S = 3/2$) (ref. 19). The determined $1 \mu_B$ in $V(\text{TCNE})_x$ indeed suggests that all spins in V^{II} ions and $(\text{TCNE})^-$ anions have collinear alignments respectively. This material can also be grown as a thin film by low-temperature (40°C) chemical vapour deposition²¹ (CVD). Although the CVD film of $V(\text{TCNE})_x$ is not crystalline, extended X-ray absorption fine-structure studies show homogeneous octahedral coordination of six nitrogens around each vanadium, with a V–N length of $2.084(5) \text{ \AA}$ (ref. 22).

Besides its robust room-temperature magnetic ordering, $V(\text{TCNE})_x$ also has a unique electronic structure, as it is proposed to be half-semiconductor-like¹³, that is, fully spin-polarized valence and conduction bands. Figure 1 shows a schematic view of the proposed spin-resolved electronic structure of $V(\text{TCNE})_x$ (ref. 13) with a modification based on surface analyses^{14,15,23}. Owing to on-site Coulomb repulsion (U_c) within $(\text{TCNE})^-$ anions, the π^* levels of $(\text{TCNE})^-$ anions split into two sublevels, one occupied (π^*) and the other empty ($\pi^* + U_c$), with opposite spin polarizations. The splitting (U_c) was estimated to be ~ 2 eV (ref. 23). The occupied $3d$ levels of V^{II} lie inside the Hubbard gap 1.5 eV above the π^* levels and 0.5 eV below the $\pi^* + U_c$ levels of $(\text{TCNE})^-$ as derived from resonant photoemission results¹⁴. The temperature dependence of the conductivity in $V(\text{TCNE})_x$ film is well described by Arrhenius law with an activation energy of ~ 0.5 eV at room temperature¹³. Magnetic circular dichroism^{14,15} and spin-polarized photoemission spectroscopy¹⁶ in metal-(TCNE) magnets support the presence of non-overlapping spin-polarized bands in these materials.

Recent spintronic research has focused on integrating control of electron spin into conventional semiconductor electronics². Intensive efforts over the past decade have been made to develop room-temperature magnetic semiconductors following theoretical prediction³. One of the main impetuses to develop a magnetic semiconductor is to avoid the conductivity mismatch problem²⁴ for efficient spin injection at the interface. Organic-based magnets such as $V(\text{TCNE})_x$ may represent an alternative to dilute magnetic semiconductors because of the demonstrated coexistence of both semiconductor character and magnetic ordering at room temperature. Meanwhile, there is increasing research activity in carbon-based spintronics. Exploration of π -conjugated organic

¹Department of Physics, The Ohio State University, Columbus, Ohio 43210-1117, USA, ²Department of Chemistry, The Ohio State University, Columbus, Ohio 43210-1173, USA, ³Chemical Physics Program, The Ohio State University, Columbus, Ohio 43210-1106, USA, ⁴Department of Materials Science and Engineering, University of Wisconsin-Madison, Madison, Wisconsin 53706-1595, USA. *e-mail: epstein@mps.ohio-state.edu.

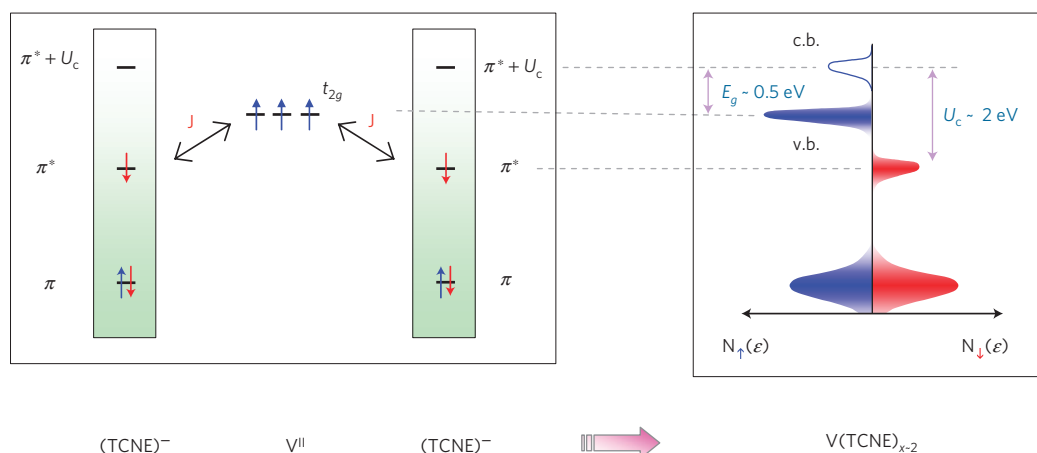


Figure 1 | Schematic view of a density of states in the organic-based magnetic semiconductor $V(TCNE)_x$. On the basis of X-ray, electron and neutron spectroscopies^{14,15,20,22,23}, it is determined that the valence band (v.b.) of $V(TCNE)_x$ is derived from the $3d(t_{2g})$ levels of vanadiums and the conduction band (c.b.) stems from the $\pi^* + U_c$ levels of TCNEs. The density of states in $V(TCNE)_x$ features highly spin-polarized valence and conduction bands with the same spin orientation and non-overlapping spin-polarized bands.

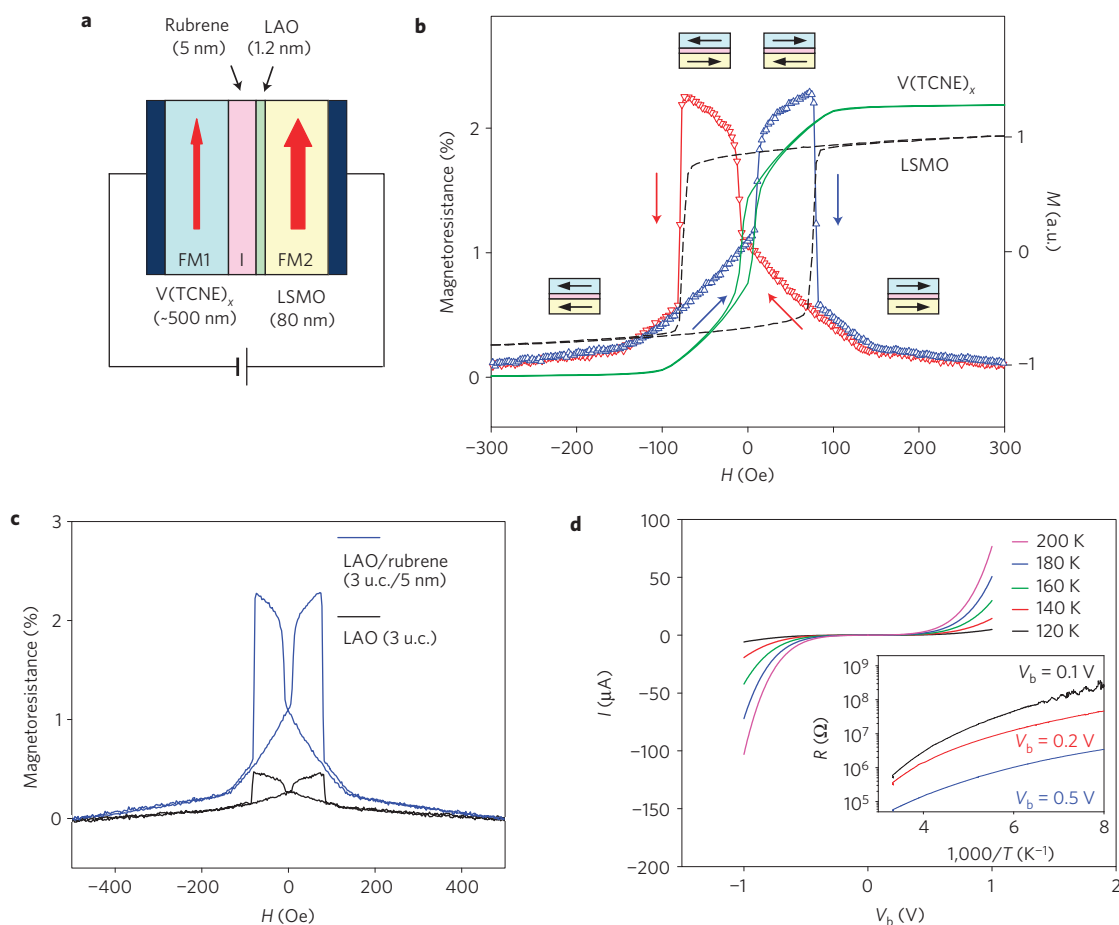


Figure 2 | Magnetoresistance and device characteristics of a hybrid magnetic tunnel junction. **a**, Schematic view of a hybrid magnetic tunnel junction of $V(TCNE)_x$ /rubrene/LAO/LSMO. The two ferromagnetic layers of different coercivity H_{c1} and H_{c2} are decoupled by the hybrid barrier of rubrene/LAO. **b**, The magnetoresistance curves of a $V(TCNE)_x$ (500 nm)/rubrene(5 nm)/LAO(1.2 nm)/LSMO(80 nm) junction measured at 100 K with a bias field of 0.5 V. The blue (red) line and uptriangles (downtriangles) are the data collected with increasing (decreasing) field. The magnetizations of $V(TCNE)_x$ (500 nm) and LSMO (80 nm) on pseudo-cubic (001) $NdGaO_3$ substrate are measured from individual films by SQUID magnetometry. **c**, The magnetoresistance curves of a magnetic tunnel junction ($V(TCNE)_x$ /insulator/LSMO) for a hybrid insulating barrier (rubrene(5 nm)/LAO(1.2 nm)) and a single LAO insulating barrier (LAO(1.2 nm)) at 100 K with a bias field of 0.5 V. **d**, The I - V curves for a hybrid magnetic tunnel junction of $V(TCNE)_x$ /rubrene/LAO/LSMO are strongly nonlinear and temperature dependent. Inset: Temperature-dependent device resistance of the hybrid magnetic tunnel junction for biases of 0.1, 0.2 and 0.5 V.

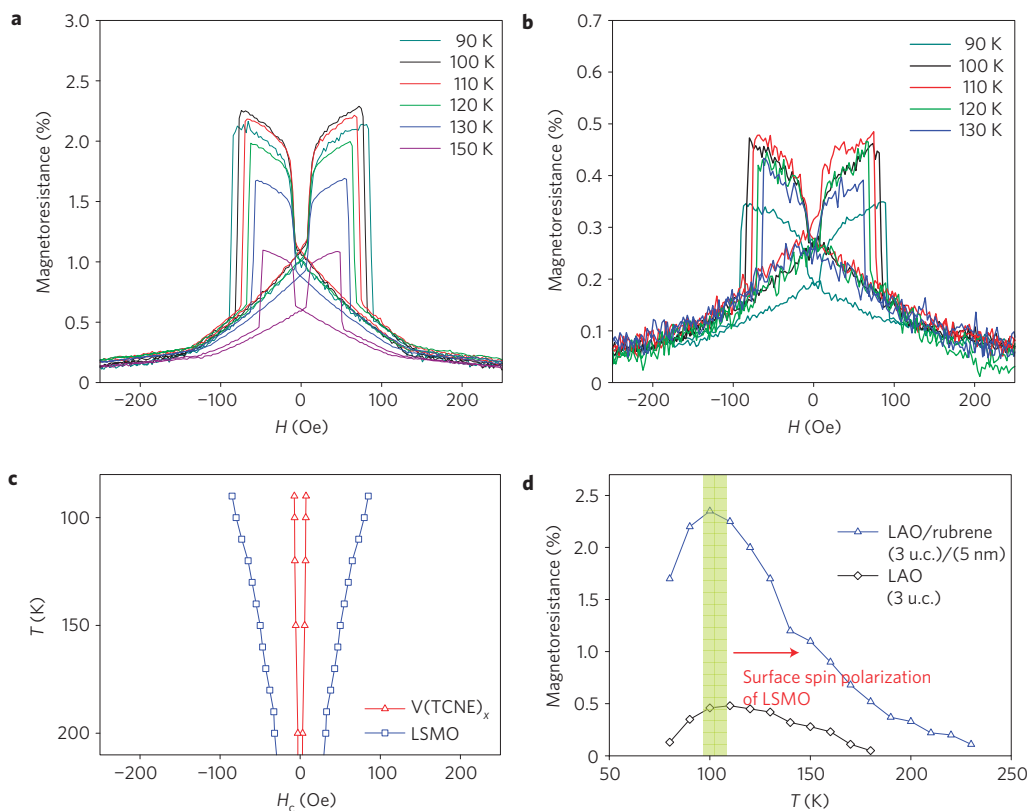


Figure 3 | Temperature dependence of magnetoresistance. **a**, The magnetoresistance curves of a hybrid magnetic tunnel junction of $V(\text{TCNE})_x(500 \text{ nm})/\text{rubrene}(5 \text{ nm})/\text{LAO}(1.2 \text{ nm})/\text{LSMO}(80 \text{ nm})$ at different temperatures with a bias field of 0.5 V. **b**, The magnetoresistance curves of a hybrid magnetic tunnel junction of $V(\text{TCNE})_x(500 \text{ nm})/\text{LAO}(1.2 \text{ nm})/\text{LSMO}(80 \text{ nm})$ at different temperatures with a bias field of 0.5 V. **c**, H_c versus T for both $V(\text{TCNE})_x(500 \text{ nm})$ and $\text{LSMO}(80 \text{ nm})$ magnetic layers. H_c is determined from individual magnetic films by SQUID magnetometry. The steps of each magnetoresistance curve correspond well to the coercivities of $V(\text{TCNE})_x(500 \text{ nm})$ and $\text{LSMO}(80 \text{ nm})$ films over all temperatures. **d**, Magnetoresistance as a function of T for both a hybrid barrier (rubrene/LAO) and a LAO barrier, with a bias field of 0.5 V. The magnetoresistance is determined from the resistance at peaks (antiparallel) and the resistance at $H = 500 \text{ Oe}$ (parallel). The magnitude of the magnetoresistance increases as T is reduced owing to the increase in surface polarization of the LSMO film and shows a maximum value at around 100 K. The decrease in magnetoresistance below 100 K can be attributed to the high bulk resistance of $V(\text{TCNE})_x$ film at low T (Supplementary Fig. S5).

materials^{5–11} as a medium of spin transport introduces a new phase of organic electronic research following successful applications of organic light-emitting diodes and organic field-effect transistors. Generally, the spins in carbon-based materials are perceived to have a long lifetime because of the extremely low spin–orbit coupling and weak hyperfine interaction. The application of organic-based magnets in spintronics offers several advantages. Among these are the unique spin-polarized semiconducting electronic structure, modulations of magnetic/electronic properties by chemical methodologies, and low-temperature processing. In addition, many of these materials exhibit magnetic bistabilities, which are often controlled by optical excitations as well as other external stimuli²⁵. Indeed, $V(\text{TCNE})_x$ film also shows a light-induced change of both magnetization and conductivity²⁶.

In this study, we demonstrate that the room-temperature organic-based magnetic semiconductor $V(\text{TCNE})_x$ functions well as the ferromagnetic layer in a hybrid magnetic tunnel junction device. Figure 2a shows a schematic view of our hybrid magnetic tunnel junction (see Supplementary Methods). An epitaxial $\text{La}_{2/3}\text{Sr}_{1/3}\text{MnO}_3$ (LSMO) thin film was employed as a second ferromagnetic layer to detect spin-polarized tunnel current from $V(\text{TCNE})_x$ as the LSMO films have been widely used in various organic/inorganic hybrid magnetic devices^{6–8,11}. Three different types of barrier, a thin oxide (1.2 nm), a thin organic semiconductor layer (5 nm) and an oxide/organic semiconductor (1.2 nm/5 nm) hybrid barrier, were studied as tunnelling barriers. The rubrene

($\text{C}_{42}\text{H}_{28}$) small-molecule thin film was used for the organic semiconducting barrier as it was shown to be highly efficient for spin-polarized tunnelling⁹. For our 5 nm rubrene spaced devices, the tunnelling current dominates the device current across the barrier as seen in comparison with the carrier injection and transport limit in rubrene spaced spin-valve devices¹¹. We employed a three-unit-cell layer of LaAlO_3 (LAO) as the thin oxide barrier. Insertion of this ultrathin oxide insulating layer (1.2 nm) excludes the formation of a dipolar barrier at the metal/organic interface, which might interfere with spin-conserved tunnelling¹⁰. In addition, capping with a thin LAO layer results in superior protection of surface polarization of the LSMO film than capping with a thin SrTiO_3 layer²⁷. The device resistance for each type of barrier varies by nearly one order of magnitude, which is a typical spread for tunnel junctions. The devices with a hybrid barrier usually have a higher magnetoresistance and a higher resistance than single-LAO-barrier devices (see Supplementary Fig. S3). However, at low T typically below $\sim 100 \text{ K}$, the bulk resistance of $V(\text{TCNE})_x$ seems to control the total resistance of the devices (Supplementary Fig. S5).

Figure 2b shows typical magnetoresistance curves for an in-plane magnetic field in the hybrid magnetic tunnel junction of $V(\text{TCNE})_x(500 \text{ nm})/\text{rubrene}(5 \text{ nm})/\text{LAO}(1.2 \text{ nm})/\text{LSMO}(80 \text{ nm})$ at 100 K with an applied bias of 0.5 V. All magnetoresistance curves in this Letter are raw experimental data without any averaging. The magnetization curves for individual magnetic layers of $V(\text{TCNE})_x$

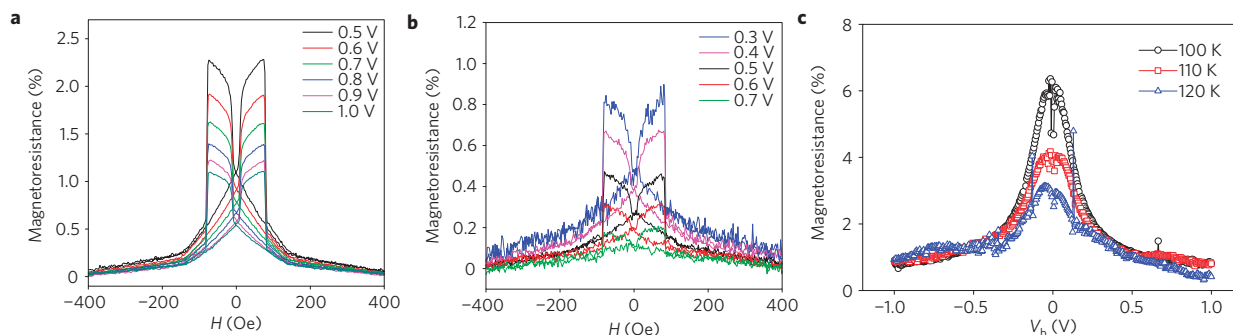


Figure 4 | Bias dependence of magnetoresistance. **a**, Magnetoresistance curves for a hybrid magnetic tunnel junction of $V(\text{TCNE})_x/\text{rubrene}/\text{LAO}/\text{LSMO}$ at 100 K for different applied biases. The steps of the magnetoresistance curves are well reproducible for each measurement at different biases. **b**, Magnetoresistance curves for a hybrid magnetic tunnel junction of $V(\text{TCNE})_x/\text{LAO}/\text{LSMO}$ at 100 K for different applied biases. **c**, The magnetoresistance as a function of V_b at $T = 100, 110$ and 120 K for a hybrid barrier (rubrene/LAO) device. Each curve is determined from the difference in the I - V curves for parallel (at 500 Oe) and antiparallel (at -60 Oe) alignments.

and LSMO films were recorded by superconducting quantum interference device (SQUID) magnetometry and are overlaid on Fig. 2b. The tunnelling current in magnetic tunnel junction devices is proportional to the sum of the products of the densities of states of the two ferromagnetic layers for each spin orientation, up and down, respectively. A higher tunnelling rate occurs when the spins of higher density of states at or close to the Fermi energy in both magnetic layers are parallel. Therefore, the device resistance changes with respect to the parallel and antiparallel configurations controlled by an external magnetic field. The magnetoresistance is defined here as $\text{MR} = (R_{\text{AP}} - R_{\text{P}})/R_{\text{P}}$, where R_{P} and R_{AP} are the device resistance for parallel and antiparallel alignments, respectively. The LSMO film has a higher density of states for majority spins at the Fermi energy as shown by spin-resolved photoemission²⁸. For $V(\text{TCNE})_x$, the electronic structure has a unique spin-polarized structure as shown in Fig. 1. The carriers in both the valence band and conduction band have the same polarization as the majority spins. The blue line and uptriangles represent the data recorded during a positive sweep of the magnetic field. The red line and downtriangles represent the data collected during negative field sweeping.

With sweeping of the magnetic field, the device resistance becomes higher when the magnetizations of two magnetic layers become antiparallel. The magnetoresistance curves correspond well to the magnetization steps of both $V(\text{TCNE})_x$ and LSMO films and clearly represent the shape of hysteresis curves of each individual magnetic layer. This unambiguously demonstrates spin filtering through a $V(\text{TCNE})_x$ magnetic semiconductor film, wherein spin-polarized carriers tunnel through the hybrid rubrene/LAO barrier while effectively conserving their spin polarization. In fact, the shapes of the magnetoresistance curves in our hybrid magnetic tunnel junctions are strongly contingent on the thickness of the LSMO bottom electrodes, as the domain structures of the LSMO films depend on the thickness of the films. The 80 nm LSMO films on NdGaO_3 substrates show particularly sharper steps of magnetoresistance curves as well as magnetizations (see Supplementary Fig. S6). The magnetoresistance of our hybrid magnetic tunnel junction is strongly dependent on the barrier, as shown in Fig. 2c. A substantial reduction of magnetoresistance was observed for the single thin LAO barrier, which is probably due to defects/pinholes of the thin LAO barrier. This suggests that employing double barriers more effectively decouples the two magnetic layers and mediates the spin-polarized tunnel current as previously shown for tunnelling magnetoresistance for hybrid oxide/organic semiconductor thin-film barriers^{9–11}. In addition, the effectiveness of adding thin small-molecule layers is probably in part due to efficient covering of defects

and pinholes in the thin insulating LAO barrier because these molecules tend to sit on metallic surfaces. Figure 2d shows nonlinear I - V curves for the magnetic tunnel junction of $V(\text{TCNE})_x(500 \text{ nm})/\text{rubrene}(5 \text{ nm})/\text{LAO}(1.2 \text{ nm})/\text{LSMO}(80 \text{ nm})$, which are strongly temperature dependent. The inset in Fig. 2d shows the temperature dependence of the total device resistance. At high T , carrier injection through the barrier controls the device resistance, whereas the bulk resistance of the $V(\text{TCNE})_x$ film limits the total device currents at low $T < 100$ K (see Supplementary Fig. S5).

The magnetoresistance of hybrid magnetic tunnel junctions of $V(\text{TCNE})_x/\text{barrier}/\text{LSMO}$ strongly depends on the temperature. The temperature-dependent magnetoresistance curves at an applied bias of 0.5 V are shown in Fig. 3a for a hybrid barrier (rubrene/LAO) and Fig. 3b for a single LAO barrier. Each magnetoresistance curve at a different temperature corresponds well to the coercivities of individual magnetic layers as shown in Fig. 3c. The coercivities of individual $V(\text{TCNE})_x$ and LSMO films in Fig. 3c are measured by SQUID magnetometry. Figure 3d shows the temperature-dependent magnetoresistance for both the thin hybrid barrier of rubrene/LAO and the thin LAO barrier devices. The magnetoresistance as a function of temperature shows a maximum at ~ 100 K. The decrease of magnetoresistance, as temperature increases above 100 K, is attributed to the decrease of surface spin polarization of the LSMO film²⁹. Similar temperature dependencies of magnetoresistance were commonly reported for hybrid organic/inorganic spin valves using LSMO films (Supplementary Fig. S7). This suggests that magnetoresistance at a higher temperature can be achieved in magnetic tunnel junctions with an organic-based magnet $V(\text{TCNE})_x$ in tandem with other ferromagnets. The magnetoresistance of our devices decreases as the temperature decreases below 100 K. As shown in Supplementary Fig. S5, the bulk resistance of the $V(\text{TCNE})_x$ film starts to dominate the total device resistance as T decreases below 100 K. Therefore, the decrease of magnetoresistance below 100 K is probably due to the fact that the magnetic-field-dependent interface resistance is overshadowed by the bulk resistance of the $V(\text{TCNE})_x$ film.

The bias dependence of magnetoresistance curves in our hybrid magnetic tunnel junction at 100 K is shown in Fig. 4a for a hybrid barrier and Fig. 4b for a single LAO barrier. The steps of magnetoresistance curves for each applied bias are well reproducible. Figure 4c shows the magnitude of magnetoresistance as a function of applied bias at $T = 100, 110$ and 120 K for a $V(\text{TCNE})_x(500 \text{ nm})/\text{rubrene}(5 \text{ nm})/\text{LAO}(1.2 \text{ nm})/\text{LSMO}(60 \text{ nm})$ junction device. Each curve is determined from the difference in the I - V curves between the parallel (at 500 Oe) and the antiparallel (at

–60 Oe) configurations. The bias dependence of magnetoresistance is similar to the behaviour of tunnelling magnetoresistance in typical inorganic magnetic tunnel junctions. At the lowest bias, data are noisier as the device resistance becomes high at low T and low V_b . Generally, the decrease of magnetoresistance by the application of a high voltage for a magnetic tunnel junction is attributed to the localized trap states in an amorphous barrier³⁰. The observed suppression of magnetoresistance by bias voltage in our device could also be related to the bulk resistance of $V(\text{TCNE})_x$ film. At low bias, the barrier resistance controls the device current. As the applied bias increases, the barrier resistance sharply drops and the bulk resistance of $V(\text{TCNE})_x$ starts to control the total device resistance. As a result, the effectiveness of electrical detection of spin-dependent tunnelling may be reduced as the bias is increased. The magnetoresistance at the applied bias of 0.1 V and 100 K is estimated as 4.7%, which is comparable to the values previously reported for large-scale organic semiconductor spaced spin valves using LSMO in combination with Co^{21} or Fe^{24} (Supplementary Fig. S7). The molecule/organic-based magnets are perceived to retain high spin polarization, and the efficient integration of these materials into spintronics devices will be advanced by the improvement of molecular interfacial engineering for the hybrid multilayered systems. Further developments in the precise control of film deposition will significantly reduce the effects of bulk resistance and improve the sensitivity of electrical detection of spin-dependent scattering signals at the interface because a few-nanometre thin-film magnetic layer should be sufficient to polarize injected carrier spins. The creation of such thin layers could also introduce spin-dependent resonant filtering through these spin-polarized molecular systems.

Research in the field of spintronics has evolved from metal-based to semiconductor- and carbon/molecule-based spintronics over the past decade. We presented magnetic tunnel junctions that exploit the spin polarization of an organic-based magnetic semiconductor. Our results show that molecule/organic-based magnetic material can function as a spin injector/detector for spintronics applications. This approach opens new avenues of chemical methodologies and low-temperature processing for developing organic/inorganic hybrid devices.

Received 29 December 2009; accepted 7 June 2010;
published online 18 July 2010; corrected online 23 July 2010

References

- Wolf, S. A. *et al.* Spintronics: A spin-based electronics vision for the future. *Science* **294**, 1488–1495 (2001).
- Awschalom, D. D. & Flatté, M. E. Challenges for semiconductor spintronics. *Nature Phys.* **3**, 153–159 (2007).
- Dietl, T., Ohno, H., Matsukura, F., Cibert, J. & Ferrand, D. Zener model description of ferromagnetism in zinc-blende magnetic semiconductors. *Science* **287**, 1019–1022 (2000).
- Appelbaum, I., Huang, B. & Monsma, D. J. Electronic measurement and control of spin transport in silicon. *Nature* **447**, 295–298 (2007).
- Tombros, N., Jozsa, C., Popinciuc, M., Jonkman, H. T. & van Wees, B. J. Electronic spin transport and spin precession in single graphene layers at room temperature. *Nature* **448**, 571–574 (2007).
- Hueso, L. E. *et al.* Transformation of spin information into large electrical signals using carbon nanotubes. *Nature* **445**, 410–413 (2007).
- Dediu, V., Murgia, M., Matarotta, F. C., Taliani, C. & Barbanera, S. Room temperature spin polarized injection in organic semiconductor. *Solid State Commun.* **122**, 181–184 (2002).
- Xiong, Z. H., Wu, D., Vardeny, Z. V. & Shi, J. Giant magnetoresistance in organic spin-valves. *Nature* **427**, 821–824 (2004).
- Shim, J. H. *et al.* Large spin diffusion length in an amorphous organic semiconductor. *Phys. Rev. Lett.* **100**, 226603 (2008).

- Santos, T. S. *et al.* Room-temperature tunnel magnetoresistance and spin-polarized tunneling through an organic semiconductor barrier. *Phys. Rev. Lett.* **98**, 016601 (2007).
- Yoo, J.-W. *et al.* Giant magnetoresistance in ferromagnet/organic semiconductor/ferromagnet heterojunctions. *Phys. Rev. B* **80**, 205207 (2009).
- Miller, J. S. & Epstein, A. J. Organic organometallic molecular magnetic materials—designer magnets. *Angew. Chem. Int. Ed. Engl.* **33**, 385–415 (1994).
- Prigodin, V. N., Raju, N. P., Pokhodnya, K. I., Miller, J. S. & Epstein, A. J. Spin driven resistance in organic-based magnetic semiconductor $V[\text{TCNE}]_x$. *Adv. Mater.* **14**, 1230–1233 (2002).
- Tengstedt, C., de Jong, M. P., Kancierzewska, A., Carlegrim, E. & Fahlman, M. X-ray magnetic circular dichroism and resonant photoemission of $V(\text{TCNE})_x$ hybrid magnets. *Phys. Rev. Lett.* **96**, 057209 (2006).
- Kortright, J. B., Lincoln, D. M., Edelstein, R. S. & Epstein, A. J. Bonding, backbonding, and spin-polarized molecular orbitals: Basis for magnetism and semiconducting transport in $V[\text{TCNE}]_{x \sim 2}$. *Phys. Rev. Lett.* **100**, 257204 (2008).
- Caruso, A. N. *et al.* Direct evidence of electron spin polarization from an organic-based magnet: $[\text{Fe}^{\text{II}}(\text{TCNE})(\text{NCMe})_2][\text{Fe}^{\text{III}}\text{Cl}_4]$. *Phys. Rev. B* **79**, 195202 (2009).
- De Fusco, G. C., Pisani, L., Montanari, B. & Harrison, N. M. Density functional study of the magnetic coupling in $V(\text{TCNE})_x$. *Phys. Rev. B* **79**, 085201 (2009).
- Matsuura, H., Miyake, K. & Fukuyama, H. Theory of room temperature ferromagnet $V(\text{TCNE})_x$ ($1.5 < x < 2$): Role of hidden flat bands. *J. Phys. Soc. Jpn* **79**, 034712 (2010).
- Manriquez, J. M., Yee, G. T., Mclean, R. S., Epstein, A. J. & Miller, J. S. A room-temperature molecular/organic-based magnet. *Science* **252**, 1415–1417 (1991).
- Zheludev, A. *et al.* Experimental determination of the spin density in the tetracyanoethenide free radical, $[\text{TCNE}]^{\cdot -}$, by single-crystal polarized neutron diffraction. a view of a π^* orbital. *J. Am. Chem. Soc.* **116**, 7243–7249 (1994).
- Pokhodnya, K. I., Epstein, A. J. & Miller, J. S. Thin-film $V[\text{TCNE}]_x$ magnets. *Adv. Mater.* **12**, 410–413 (2000).
- Haskel, D. *et al.* Local structural order in the disordered vanadium tetracyanoethylene room-temperature molecule-based magnet. *Phys. Rev. B* **70**, 054422 (2004).
- Tengstedt, C. *et al.* Coulomb interactions in rubidium-doped tetracyanoethylene: A model system for organometallic magnets. *Phys. Rev. B* **69**, 165208 (2004).
- Schmidt, G., Ferrand, D., Molenkamp, L. W., Filip, A. T. & van Wees, B. J. Fundamental obstacle for electrical spin injection from a ferromagnetic metal into a diffusive semiconductor. *Phys. Rev. B* **62**, R4790–R4793 (2000).
- Sato, O., Tao, J. & Zhang, Y. Z. Control of magnetic properties through external stimuli. *Angew. Chem. Int. Ed.* **46**, 2152–2187 (2007).
- Yoo, J.-W. *et al.* Multiple photonic responses in films of organic-based magnetic semiconductor $V(\text{TCNE})_x$, $x \sim 2$. *Phys. Rev. Lett.* **97**, 247205 (2006).
- Yamada, H. *et al.* Engineered interface of magnetic oxides. *Science* **305**, 646–648 (2004).
- Park, J.-H. *et al.* Direct evidence for a half-metallic ferromagnet. *Nature* **392**, 794–796 (1998).
- Park, J.-H. *et al.* Magnetic properties at surface boundary of a half-metallic ferromagnet $\text{La}_{0.7}\text{Sr}_{0.3}\text{MnO}_3$. *Phys. Rev. Lett.* **81**, 1953–1956 (1998).
- Tsymbal, E. Y., Mryasov, O. N. & LeClair, P. R. Spin-dependent tunnelling in magnetic tunnel junctions. *J. Phys. Condens. Matter* **15**, R109–R142 (2003).

Acknowledgements

We thank J. S. Miller and K. I. Pokhodnya for initial collaboration and their help in developing $V(\text{TCNE})_x$ film. This work was supported in part by AFOSR Grant No. FA9550-06-1-0175, DOE Grant Nos DE-FG02-01ER45931, DE-FG02-86ER45271, DE-FG02-06ER46327, NSF Grant No. DMR-0805220 and ONR Grant No. N00014-07-1-0215.

Author contributions

J.-W.Y., V.N.P. and A.J.E. wrote the manuscript. J.-W.Y. and A.J.E. worked on device characteristics, data collection and analysis. J.-W.Y. and C.-Y.C. did device fabrication. C.-Y.C. did CVD growth for $V(\text{TCNE})_x$ films and synthesis for the precursors of $V(\text{TCNE})_x$. H.W.J., C.W.B. and C.B.E. prepared epitaxial LSMO samples with LAO capping. All authors discussed the progress of research and reviewed the manuscript.

Additional information

The authors declare no competing financial interests. Supplementary information accompanies this paper on www.nature.com/naturematerials. Reprints and permissions information is available online at <http://npg.nature.com/reprintsandpermissions>. Correspondence and requests for materials should be addressed to A.J.E.

Spin injection/detection using an organic-based magnetic semiconductor

Jung-Woo Yoo, Chia-Yi Chen, H. W. Jang, C. W. Bark, V. N. Prigodin, C. B. Eom & A. J. Epstein

Nature Materials **9**, 638–642 (2010); published online: 18 July 2010; corrected after print: 23 July 2010.

In the original version of this article published online and in print, the received date should have been 29 December 2009, not 2010. This has been corrected in the PDF and HTML versions of this Letter.